Research Article Vol. 3, No. 3 / 15 March 2020 / OSA Continuum 568

Stability of Q-switched 2 µm lasers

JAMES BROOKS,[1,2] GERALD M. BONNER,[1,*] ALAN J. KEMP,[2] AND DAVID J. M. STOTHARD[1]

[1] *Fraunhofer CAP, Technology and Innovation Centre, 99 George Street, Glasgow G1 1RD, UK*
[2] *Institute of Photonics, Department of Physics, SUPA, University of Strathclyde, 99 George Street, Glasgow G1 1RD, UK*
[*] *gerald.bonner@fraunhofer.co.uk*

Abstract: Q-switched lasers operating at wavelengths around 2 µm have many applications including materials processing and LIDAR. However, the low gain of the quasi-three-level gain media available at 2 µm can lead to problems with pulse-to-pulse fluctuations in their output, known as jitter. Here we present a methodology for characterising the level of jitter in a Q-switched laser and apply it to a Tm:YAP system. We also look at the causes of jitter and evaluate some methods of reducing it. The methodology developed here will aid in the development and characterisation of Q-switched lasers at any wavelength.

1. Introduction

Q-switched 2 µm lasers have applications in materials processing [1] and laser surgery [2–5] due to the strong absorption of plastics and water respectively around this wavelength [1]. Lasers operating around 2 µm are useful for remote sensing [4,6,7] due to the "eye-safe" wavelength [8,9]. Depending on the sensing application, atmospheric transmission (for LIDAR) [8] or absorption features (for gas sensing, particularly H_2O and CO_2) [9] around 2 µm can be taken advantage of. Finally, 2 µm lasers can be used to pump non-linear materials to reach the 3 µm – 12 µm range [3,6,10]; this unlocks applications in spectroscopy [11,12] and defence [3,11].

Minimizing pulse-to-pulse fluctuations (jitter) is one key challenge for the commercialization of Q-switched lasers. While jitter is a well-known phenomenon, and is present to some degree in all Q-switched lasers, it is not extensively discussed in the literature. The main exception to this is research on passively Q-switched lasers; for example, Qiao *et al.* [13] and Lin *et al.* [14] briefly look into the amplitude jitter of their Tm:LuAG and Nd:YAG lasers (respectively) as part of the characterisation of new saturable absorber materials. In these works, the pulse train is recorded and the clock amplitude jitter (CAJ) is calculated according to $\mathrm{CAJ} = \sigma/M \times 100\%$ as in [15] where σ is the standard deviation and M is the mean value of the intensity.

To our knowledge, the only publication of a detailed investigation of jitter in an actively Q-switched laser was by Martin *et al.* [16]. Their analysis focused on pulse timing jitter in a single-frequency Nd:YAG laser Q-switched using an acousto-optic modulator and the pre-lase technique [17–19]. The method used in [16] centred on recording 5000 consecutive pulses and comparing the build-up times. In their analysis, evidence was found of both stochastic and oscillatory effects on the jitter; a fast Fourier transform showed the oscillatory component was at 105 Hz. A numerical model was able to reproduce the main features of the jitter and it is postulated that the periodic perturbations are due to mechanical or electrical resonances in the system.

In this paper, we present a jitter characterization process applicable to any Q-switched laser, focusing on an electro-optically Q-switched Tm:YAP system. We investigate the jitter in all pulse

#389477 https://doi.org/10.1364/OSAC.389477
Journal © 2020 Received 19 Feb 2020; accepted 21 Feb 2020; published 5 Mar 2020

OSA CONTINUUM

parameters, not just the build-up time, as well as its origins and begin an analysis of potential routes to reducing jitter.

2. Origins of jitter

In order to investigate the origins of jitter, we start with the equations describing the pulse parameters in a quasi-three-level laser material such as thulium, derived following [20]. In Eqs. (1) – (4), τ_b is the build-up time, P_p is the peak power, E_p is the pulse energy and τ_p is the pulse duration. N_i/N_p is the over-pumping ratio (a measure of how far above threshold the laser is), N_i is the population inversion density before the pulse and N_p is the value at the peak of the pulse (which is equivalent to the CW threshold value). V_a is the mode volume in the gain medium, τ_c is the cavity lifetime. $f = \sigma_a/\sigma_e$ is the ratio of the effective re-absorption and stimulated emission cross-sections, σ_a and σ_e respectively. γ_2 is the logarithmic loss due to the output coupler, A_b is the mode area and η_E is the energy utilisation factor which is a measure of how much of the energy stored in the population inversion has been extracted by the pulse. Equations 1 – 4 differ from their equivalents for a four-level system by the $\frac{1}{1+f}$ factor that acts to reduce the build-up time, peak power and pulse energy for the quasi-three-level system.

$$\tau_b = \frac{\tau_c}{N_i/N_p - 1} \ln\left[\frac{V_a N_p}{1+f}\left(\frac{N_i}{N_p} - \ln\left(\frac{N_i}{N_p}\right) - 1\right)\right] \tag{1}$$

$$P_p = \frac{\gamma_2}{2}\frac{h\nu}{\tau_c}\frac{A_b}{\sigma_e}\frac{1}{1+f}\left(\frac{N_i}{N_p} - \ln\left(\frac{N_i}{N_p}\right) - 1\right) \tag{2}$$

$$E_p = \frac{\gamma_2}{2}\frac{A_b}{\sigma_e}\frac{h\nu}{1+f}\eta_E\frac{N_i}{N_p} \tag{3}$$

$$\tau_p = \frac{E_p}{P_p} = \tau_c\frac{(N_i/N_p)\eta_E}{(N_i/N_p) - \ln(N_i/N_p) - 1} \tag{4}$$

Of all the parameters influencing the values of these four pulse parameters, only N_i, N_p and τ_c can vary on a pulse-to-pulse basis through the pump power (for N_i) and losses (for N_p and τ_c). (Here we have assumed that the cavity mode volume is constant.) In order to demonstrate how the pump power and cavity losses affect a laser's output characteristics, we plot Eqs. (1) and (4) for a range of over-pumping ratios in Fig. 1 (P_p and E_p are both almost linear with the over-pumping ratio). As the over-pumping ratio increases (ie the pump power increases and/or the cavity losses decrease), the build-up time and pulse duration decrease.

A calculation of the value of the over-pumping ratio, using Eq. (5), for the Tm:YAP laser used in this work gives a value of 9.1 for typical operating parameters; repeating the calculation for a Nd:YVO_4 laser under similar conditions gives a value of 67.2. Equation 5 is the solution to the population inversion rate equation (for a quasi-three-level system) at time $t = \tau$ before the Q-switch occurs (ie there are no photons in the cavity). R_p is the pump rate density, τ is the upper laser level lifetime, N_t is the total active ion density, γ is the logarithmic loss per pass and l is the length of the gain material. It can be seen that the considerably higher stimulated emission cross-section is a reason for the higher over-pumping ratio obtained from the Nd:YVO_4 laser.

$$\frac{N_i}{N_p} = \frac{(R_p\tau(1+f) - fN_t)(1 - e^{-1})}{\frac{\gamma}{\sigma_e l}} \tag{5}$$

In both cases, the theoretical laser was pumped at the same pump power (4 W), used the same cavity and the pump time was set equal to the material lifetime to ensure a fair comparison. Table 1 shows the values used for each parameter in calculating the over-pumping ratio for each material. Looking at Fig. 1 at these over-pumping ratio values reveals why lasers based on

OSA CONTINUUM

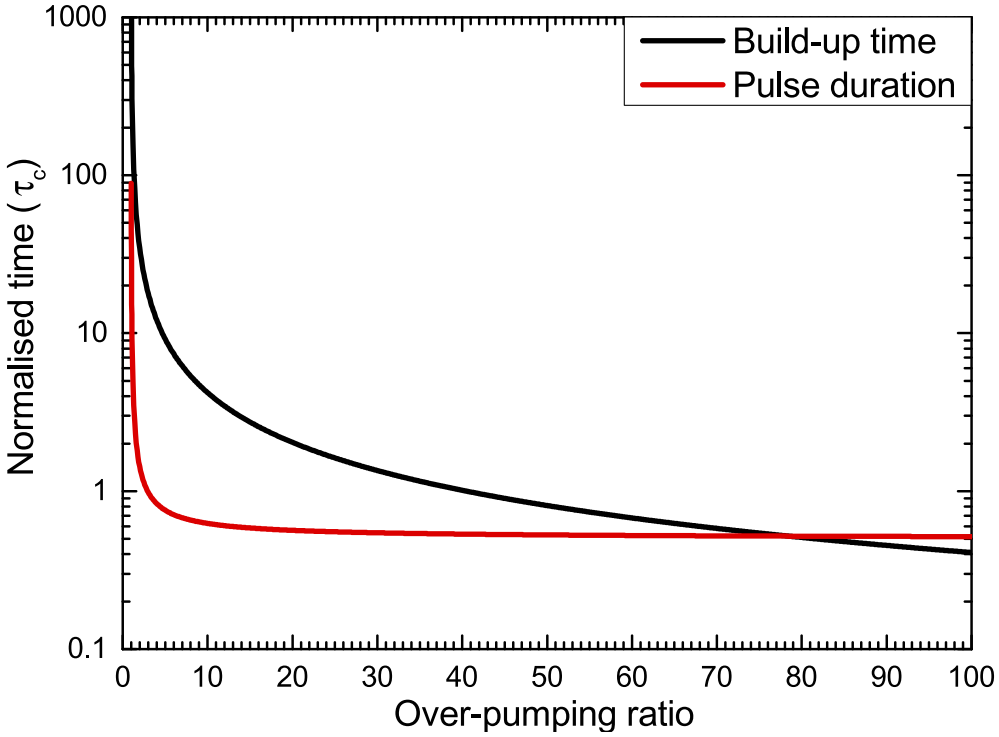

Fig. 1. Over-pumping ratio dependency of the build-up time and pulse duration for the Tm:YAP laser.

neodymium tend to have low jitter; the curves are considerably steeper in the region about 10 (where the Tm:YAP can be expected to operate) and so a small change in the over-pumping ratio will cause a large change in the pulse parameters which constitutes a large jitter. As noted above, changes in over-pumping ratio can be caused by variations in the pumping process and/or changes in the cavity loss on a pulse-to-pulse basis (including mechanical vibrations and air currents). The output of the pump diode was measured with a fast photodetector and no fluctuations above the electrical noise floor were observed. This suggests that pump instabilities are not significant and so we focus on pulse-to-pulse changes to the cavity losses. However, calculations of the build-up time (using Eq. (1)) for pump powers around 4 W show pump power fluctuations of 1 % could produce jitter in the build-up time of 1.3 % (this assumed everything else was constant).

It should be noted that the over-pumping ratio could not be experimentally defined as there is no way to measure the population inversion before the pulse (N_i). In calculating the over-pumping ratios above, it was assumed that the system started with no population inversion before the pump phase. In reality, a Q-switched pulse cannot sweep out all of the gain stored in the medium and so some population inversion will be left at the start of the pump phase. This starting population inversion becomes more important at higher repetition rates where there is less pumping time and so N_i could be very different for consecutive pulses. As we are not currently aware of a method of reliably measuring the population inversion during Q-switched operation in a quasi-three-level material, values for the over-pumping ratio cannot be given for the experiments undertaken. As a rule of thumb, a higher over-pumping ratio can be attained by operating at a higher pump power and lower repetition rate.

OSA CONTINUUM

Table 1. Parameters used to generate Fig. 1 and calculate the over-pumping ratios of the Tm:YAP laser used in this work and a Nd:YVO_4 under similar conditions. Unreferenced values are either calculated (equation given) or describe the modelled cavity.

Parameter	Nd:YVO_4 [ref.]	Tm:YAP [ref.]
λ_L (nm)	1064	1940
ω (μm)	140	140
l (mm)	3	3
$V_a = \pi\omega^2 l$ (10^{-10} m)	1.85	1.85
γ	0.0357	0.0357
$\sigma_e(\lambda_L)$ (cm^2)	1.44×10^{-18} [21]	5×10^{-21} [22]
$\sigma_a(\lambda_L)$ (cm^2)	0	0.486×10^{-21} [22]
$f = \frac{\sigma_a}{\sigma_e}$	0	0.0972
τ (μs)	100 [23]	4400 [24]
N_t @ 4 at.%Tm (m^{-3})	–	7.86×10^{26} [25]
λ_p (nm)	808.5 [23]	795 [2]

3. Method

3.1. Experimental setup

A diagram of the test laser created for this work is shown in Fig. 2. The pump source used is a DILAS fibre-coupled 795 nm 25 W diode laser (model number M1F2S22-795.3-25C-SS2.1). The pump light is delivered to the breadboard by a 200 μm diameter core, 0.22 numerical aperture fibre. The beam is collimated by a 35 mm focal length lens and then enters a variable attenuator. The attenuator comprises two polarising beamsplitters and a half-wave plate as shown. Rotation of the half-wave plate allows the selection of a pump power while keeping the diode current and temperature (and hence wavelength and mode content) constant. The attenuated pump beam then passes through a 30:70 (R:T) non-polarising beamsplitter, which allows monitoring of the unabsorbed pump, before being focussed by a 50 mm focal length lens to a spot radius of ~140 μm at the centre of the crystal (measured using the knife-edge technique). The use of the attenuator limited the maximum pump power usable during these experiments due to the first polariser immediately rejecting half of the unpolarised pump power, the non-polarising beamsplitter removing another 30 % and losses at surfaces further reducing the transmitted power. The maximum pump power through the attenuator setup was measured to be 7.5 W. Around 90 % of the incident pump power was absorbed after the double-pass of the crystal.

The crystal used was an *a*-cut (P_{nma} notation) 4 at% Tm:YAP from Scientific Materials with dimensions of 4 mm×4 mm×3 mm. The crystal is coated on one side to be HR at the laser wavelength ($T < 0.2\%$ @ 1940 nm and 1990 nm) and HT at the pump wavelength ($T > 99\%$ @ 793 nm – 795 nm), with the other side vice versa ($T > 99.4\%$ @ 1940 nm and 1990 nm and $T < 1.2\%$ @ 793 nm – 795 nm). Following the crystal are two infrasil lenses with focal lengths of −50 mm and 50 mm to make the cavity mode as collimated as possible in the next part of the cavity. Following the lenses is a thin-film polariser from LAYERTEC designed for use at Brewster's angle. The polariser is coated to be highly reflective for the S-polarisation (in this case vertically out of the page and optical bench). After the polariser are two Pockels cells supplied by Cristal Laser, each cell is made up of a pair of 3 mm×3 mm×5 mm RTP crystals which are AR coated for the laser wavelength around 1940 nm (there are two Pockels cells as the laser was designed to be capable of cavity-dumping). Next is a zero-order quarter-wave plate from Thorlabs designed for operation at 2020 nm but suitable for use at 1940 nm. Next is space for two uncoated YAG etalons (LightMachinery) with thicknesses of 5 mm and 0.25 mm. Finally, there is a plane output coupler to complete the cavity. Output coupler transmissions of 5 %, 10 %

OSA CONTINUUM

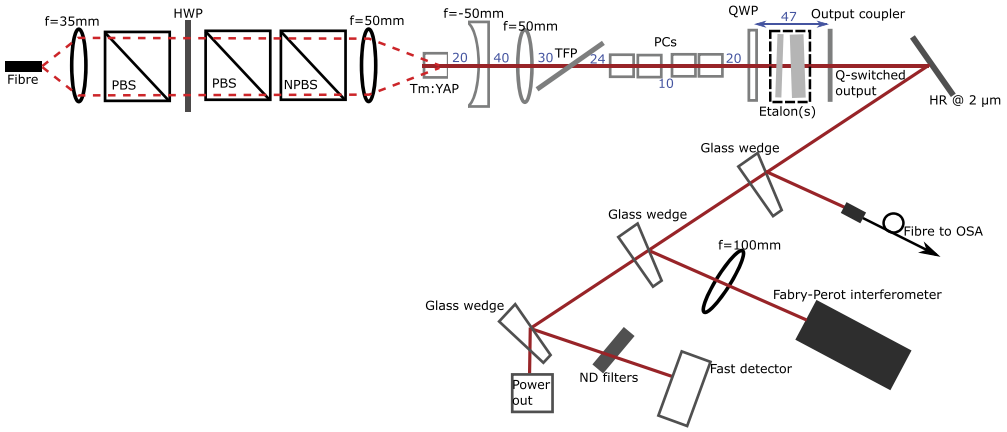

Fig. 2. Diagram of cavity and diagnostics used throughout this work. PBS = polarising beamsplitter, NPBS = non-polarising beamsplitter, HWP = half-wave plate, TFP = thin-film polariser, PCs = Pockels cells, QWP = quarter-wave plate. Optic spacings in mm are shown in blue. There is a 3 mm gap between the crystals that make up each Pockels cell.

and 20 % were used in this work. The laser is operated with continuous pumping; therefore, any mention of repetition rate refers to the Q-switching.

3.2. Jitter characterisation process

In order to assess the level of jitter in a given laser system, we record a large number (2500 or enough to fill memory) of consecutive pulses using a fast photodetector (EOT5000, bandwidth >12.5 GHz, rise- and fall-time 28 ps) and oscilloscope (Rohde & Schwarz RTO 1044). The oscilloscope's ultra-segmentation mode was used to minimize the blind time between acquisitions and enable the recording of consecutive pulses; this is important to get a true indication of the jitter. We also record the average output power of the laser with a thermal power meter (Thorlabs S310C).

The recorded pulses are then analysed by a MATLAB script that calculates the build-up time, pulse duration, peak power and pulse energy for each pulse as follows, shown graphically in Fig. 3. The build-up time was taken as the time period between the peak of the high-voltage noise picked up by the photodetector due to the activation of the Pockels cell and the peak of the optical pulse. The high-voltage noise was used as it is the time at which the Pockels cell activates; therefore, measuring from this time gives the true build-up time as the time between the losses being switched and the peak of the pulse. The pulse duration was defined as the full width at half maximum (FWHM) of the Q-switched pulse. The peak power and pulse energy require the conversion from the oscilloscope y-axis of volts to power in watts. This was done by defining a conversion factor $C = \frac{P_{avg}}{F \times A_{avg}}$ where P_{avg} is the average power measured using the thermal power meter, F is the repetition rate and A_{avg} is the average area under the pulse (not the beam area). The area under each pulse is calculated by numerical integration in the script. Using this factor, the peak power (in W) is calculated as the peak value of the pulse (in V) multiplied by the conversion factor and the pulse energy (in J) is the area under the pulse (in V s) multiplied by the conversion factor.

Once the pulse parameter values are known for each pulse, the script calculates the mean (μ) and standard deviation (σ) for each parameter. The percentage jitter in parameter x is then calculated using $\Delta x = \frac{3\sigma_x}{\mu_x} \times 100$. This definition captures the range of a given parameter for the

OSA CONTINUUM

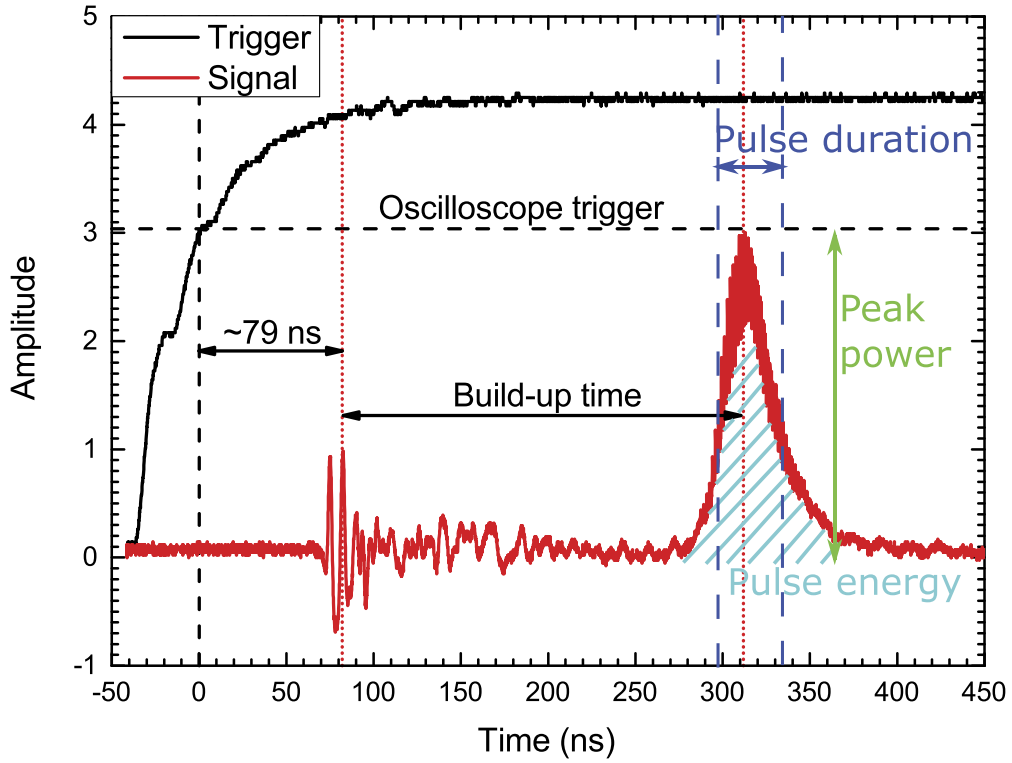

Fig. 3. Example pulse showing definitions of pulse parameters discussed in this paper. The build-up time is the time between the peak of the high-voltage noise and the peak of the pulse. The pulse duration is the FWHM of the pulse. The peak power is the height of the peak and the pulse energy is the area under the peak (both of these require conversion from oscilloscope units).

99.7 % of events that lie within 3σ either side of the mean. We take two runs of data for each operating condition we test and average the jitter values from the two runs.

4. Results

In this section, we present the results of the jitter characterisation on the laser under different conditions. First, we look at the effect of pump power, repetition rate and output coupling on a breadboard system. Next, we investigate the role of mode competition in jitter and, finally, we examine the effect of mechanical stability.

4.1. Breadboard system

In this section, we analyse the jitter for the cavity without etalons under different combinations of pump power (between 1.9 W and 7.1 W), repetition rate (50 Hz – 5000 Hz) and output coupler (5 %, 10 % and 20 %). First, we plot figures such as that shown in Fig. 4(a) and note that there does not appear to be any pattern to the jitter in time; the pulse parameters are approximately normally distributed about the mean value, as shown in Fig. 4(b).

Next we use the script described above to analyse the jitter in the laser under different operating conditions. Figure 5(a) shows the percentage jitter in all parameters against the incident pump power, for fixed repetition rate of 250 Hz and 5 % output coupler. It can be seen that the jitter

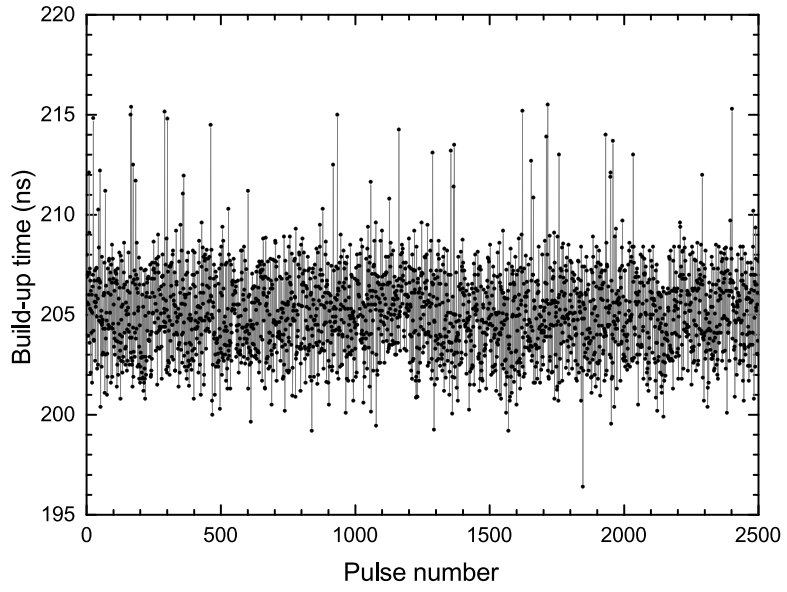

(a)

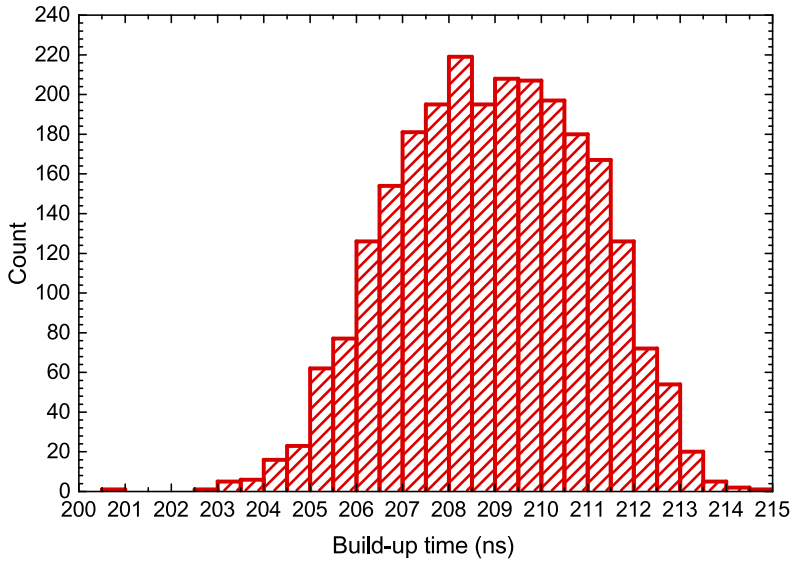

(b)

Fig. 4. (a) Build-up time of each pulse and (b) histogram of the build-up times with the 5 % output coupler, operating at 250 Hz repetition rate and 4:9 W incident pump power in order showing no pattern in the jitter.

OSA CONTINUUM

is reduced at higher pump powers, this is expected as increasing the pump power increases the over-pumping ratio which should reduce the jitter as postulated in section 2. Figure 5(b) shows the dependence of the jitter on the repetition rate for fixed pump power of 4.9 W and the same output coupler. Here, we note that the jitter is an order of magnitude higher at 5 kHz compared to the other repetition rates; this is due to the higher repetition rate decreasing the available pump time which will lead to a lower initial population inversion (at the same pump power) and therefore a lower over-pumping ratio.

Finally, the effect of the output coupling on the jitter will be examined. Table 2 shows the percentage jitter of each parameter for each output coupler for the case of a repetition rate of 250 Hz and incident pump power of 4.9 W. From this table, it can be seen that the jitter is worse with the 20 % output coupler as, taking the average of the two runs, the standard deviation and percentage jitter in each parameter increases with output coupling. This is expected as a higher output coupling means greater losses in the cavity which leads to a lower over-pumping ratio (for the same pump power and pumping time) and therefore more jitter.

Table 2. Jitter in all pulse parameters as the output coupler is changed with the same pump power of 4.9 W and repetition rate of 250 Hz.

Output coupler	$\Delta\tau_b$ (%)	$\Delta\tau_p$ (%)	ΔP_p (%)	ΔE_p (%)
5 %	2.8	13	20	6.9
10 %	3.2	28	22	12
20 %	6.6	17	32	13

From these results, we see that the jitter in the laser follows the theory set out in section 2; operating at higher over-pumping ratios (attained by increasing the pump power, reducing the repetition rate or output coupling) reduces the jitter. We now look at other potential causes of jitter.

4.2. Mode control

It has been shown that the instabilities seen in passively Q-switched two-mode microchip lasers are due to longitudinal-mode competition [26]. We therefore move to investigate the effect of mode content on jitter. To this end, we include the two YAG etalons (thicknesses 5 mm and 0.25 mm) in the cavity and compare to data taken immediately prior to adding the etalons (note that the laser was re-aligned for this data). Upon inserting these, the jitter became considerably worse as can be seen when comparing the few mode cases to the without etalons case in Table 3. We propose that the reason for this is that mode competition effects are becoming worse as the mode content is restricted and that these effects are a cause of jitter. We posit that this is analogous to the CW case where reduced mode content (towards 2 modes) causes intensity fluctuations that become more severe as the number of modes is reduced; in the CW case, these fluctuations are eliminated when single-mode operation is achieved.

Table 3. Summary of results of jitter analysis for the cases described in sections 4.2 and 4.3 with the laser operating with 4.9 W pump power, 250 Hz repetition rate and with the 5 % output coupler.

Case	$\Delta\tau_b$ (%)	$\Delta\tau_p$ (%)	ΔP_p (%)	ΔE_p (%)
Without etalons	2.5	1.3	3.2	2.8
4 modes	6.4	2.8	7.9	5.1
3 modes	7.2	2.8	5.9	3.5
2 modes	7.2	2.2	5.0	5.0
Mechanically robust	1.1	2.0	3.8	2.6
Mechanically robust with etalons	7.3	8.5	8.3	5.4

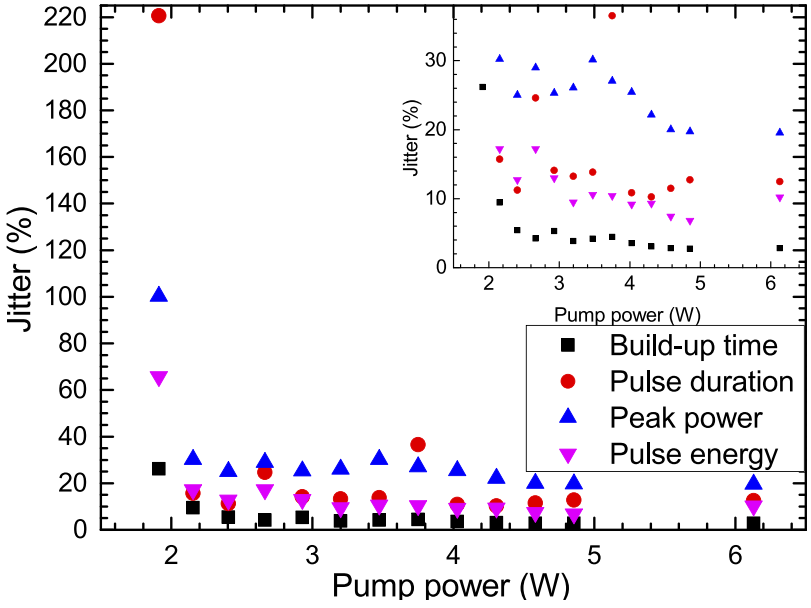

(a)

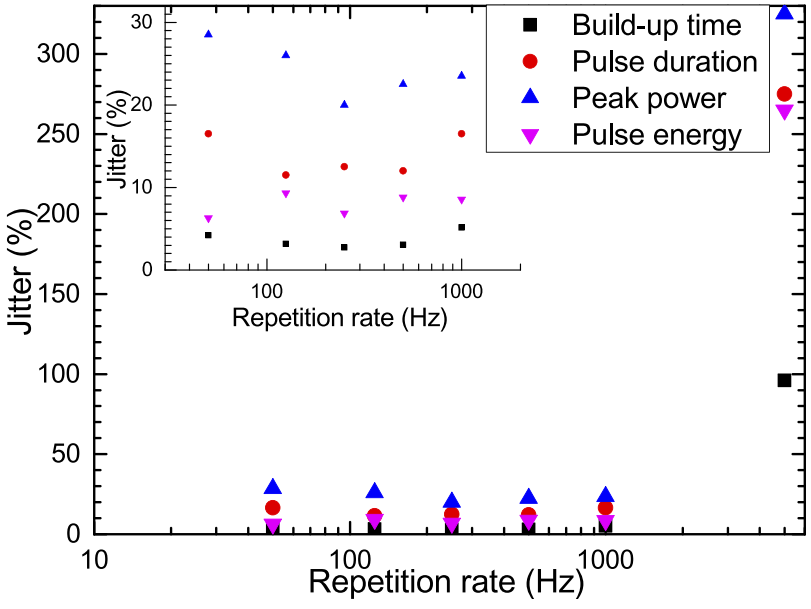

(b)

Fig. 5. (a) Effect of pump power on the percentage jitter in the pulse parameters for 250 Hz repetition rate and 5 % output coupler. (b) Effect of repetition rate on the percentage jitter in the pulse parameters for 4.9 W incident pump power and 5 % output coupler. The insets show a zoom in on the lower jitter values.

OSA CONTINUUM

In order to test this, we used the etalons to enforce laser operation on 4, 3 and 2 adjacent modes (oscillation was not possible on a single-longitudinal-mode nor > 4 adjacent modes). We used a scanning Fabry-Perot interferometer (free-spectral range 10 GHz) to observe the mode content of the laser and an optical spectrum analyser (maximum resolution 10 GHz) to ensure the modes are adjacent. A bespoke, ultra-high bandwidth boxcar integrator was used in conjunction with the interferometer to allow us to build up the spectrum over multiple pulses.

We measured the jitter for each of 4, 3 and 2 modes (non-consecutively) with the laser again operating at a repetition rate of 250 Hz, incident pump power of 4.9 W and the 5 % output coupler. The results are shown in Table 3. The build-up time results show some evidence for jitter getting worse as the number of modes decreases but it is not conclusive; more data points are needed to confirm the trend.

In an effort to enforce single-longitudinal-mode operation, we implemented a version of the pre-lase technique [17–19]. In this technique, the losses are slightly reduced to allow a single mode to oscillate and seed the main pulse. Our implementation of pre-lase increased the jitter due to the seed pulse (essentially the first relaxation oscillation) being, deliberately, generated with a very low over-pumping ratio. Therefore, our seed pulse introduced a large jitter to the system. We suggest a more advanced implementation of pre-lase using a PID loop to force the seed pulse to become a CW level (as in [27]) could be a promising route to low-jitter single-frequency operation.

4.3. Mechanical stability

We now address mechanical vibrations as a cause of jitter identified in section 2 by switching from the breadboard laser to a more robust housing. This was designed to reduce the number of degrees of freedom on as many components as possible while retaining enough to facilitate alignment. Water cooling was swapped for TEC cooling with a heat pipe. A photo of the system is shown in Fig. 6. The mechanically stabilized system was tested with and without etalons in the cavity (etalons show in position in Fig. 6).

As previously, we measure the jitter for an incident pump power of 4.9 W, repetition rate of 250 Hz and 5 % output coupler. We compare the jitter values obtained with those from the breadboard system in Table 3 (first and second last rows) and note that the percentage jitter has been reduced in all parameters. We infer that a main cause of jitter in this system is mechanical vibration in the post-mounted breadboard implementation. We acknowledge that more could be done with this ruggedised housing to improve upon this implementation; this may further reduce the jitter. Further improvements would reduce the degrees of freedom further and could include fixing optics with an adhesive and removing the rotation on the crystal mount.

Following this, the etalons for longitudinal mode control were introduced to the cavity. As in section 4.2, single-frequency operation could not be enforced without the pre-lase technique (causing the same issues described previously). The addition of the etalons lead to an increase in the jitter in all parameters to similar levels as when using the etalons with the breadboard laser (see Table 3). From this we conclude that mode competition effects dominate over mechanical stability when operating on few longitudinal modes.

In addition to improving the mechanical stability, the new cavity was designed to allow purging of the cavity to reduce the effects of atmospheric water absorption at this wavelength [1]. A dry air purge was able to reduce the relative humidity in the cavity from 33 % to 5 %. However, no significant effect on the already low jitter in the mechanically-stabilised system was observed. This leads us to the conclusion that other jitter causes are more significant.

OSA CONTINUUM

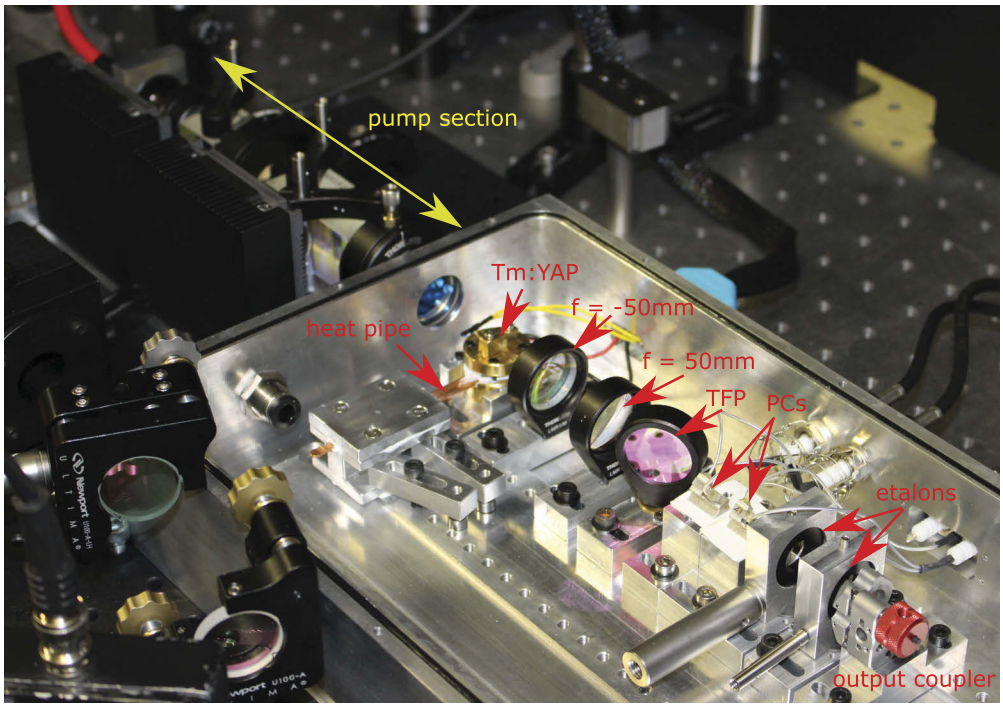

Fig. 6. Photo of ruggedised system.

5. Conclusions

In summary, we have developed a methodology to characterise the jitter in a Q-switched laser. This analysis has shown that the jitter is worse at lower pump powers, higher repetition rates and higher output couplings. The first two of these are linked to reduced initial population inversion and the last to increased losses, these both contribute to decreasing the over-pumping ratio that the laser is operating at. We have presented some evidence that reducing the mode content of the laser towards 2 adjacent longitudinal modes leads to increased jitter. We have also shown that improving the stability of the cavity reduces the jitter in all pulse parameters.

These experiments have confirmed the link between low over-pumping ratio and increased jitter and have also shown that mechanical vibrations are a main cause of jitter. The best ways to reduce jitter are to operate at higher pumping powers, lower repetition rates and with lower output couplings in a mechanically robust cavity that offers minimal degrees of freedom on optics. Further investigation is required to confirm the link between mode content and jitter; this will require methods of enforcing laser oscillation on greater numbers of adjacent longitudinal modes as well as single-frequency operation.

Funding

Engineering and Physical Sciences Research Council (EP/L01596X/1); Royal Academy of Engineering (10145-101).

Acknowledgments

We would like to thank Keith Oakes of Elforlight Ltd. for the loan of a Pockels cell.

OSA CONTINUUM

Disclosures

The authors declare that there are no conflicts of interest related to this article.

References

1. M. Eichhorn, "Quasi-three-level solid-state lasers in the near and mid infrared based on trivalent rare earth ions," Appl. Phys. B **93**(2-3), 269–316 (2008).
2. R. C. Stoneman and L. Esterowitz, "Efficient 1.94 µm Tm:YALO laser," IEEE J. Sel. Top. Quantum Electron. **1**(1), 78–81 (1995).
3. E. C. Honea, R. J. Beach, S. B. Sutton, J. A. Speth, S. C. Mitchell, J. A. Skidmore, M. A. Emanuel, and S. A. Payne, "115-W Tm:YAG diode-pumped solid-state laser," IEEE J. Quantum Electron. **33**(9), 1592–1600 (1997).
4. B. M. Walsh, "Review of Tm and Ho materials; spectroscopy and lasers," Laser Phys. **19**(4), 855–866 (2009).
5. N. Fried, "Recent advances in infrared laser lithotripsy," Biomed. Opt. Express **9**(9), 4552–4568 (2018).
6. S. R. Bowman, J. G. Lynn, S. K. Searles, B. J. Feldman, J. McMahon, W. Whitney, D. Epp, G. J. Quarles, and K. J. Riley, "High-average-power operation of a Q-switched diode-pumped holmium laser," Opt. Lett. **18**(20), 1724–1726 (1993).
7. R. C. Stoneman and L. Esterowitz, "Efficient, broadly tunable, laser-pumped Tm:YAG and Tm:YSGG cw lasers," Opt. Lett. **15**(9), 486–488 (1990).
8. S. W. Henderson, P. J. M. Suni, C. P. Hale, S. M. Hannon, J. R. Magee, D. L. Bruns, and E. H. Yuen, "Coherent laser radar at 2 µm using solid-state lasers," IEEE Trans. Geosci. Remote Sensing **31**(1), 4–15 (1993).
9. Q. Wang, J. Geng, and S. Jiang, "2 µm fiber laser sources for sensing," Opt. Eng. **53**(6), 061609 (2013).
10. P. A. Budni, L. A. Pomeranz, M. L. Lemons, C. A. Miller, J. R. Mosto, and E. P. Chicklis, "Efficient mid-infrared laser using 1.9 µm-pumped Ho:YAG and $ZnGeP_2$ optical parametric oscillators," J. Opt. Soc. Am. B **17**(5), 723–728 (2000).
11. P. Černý and D. Burns, "Modeling and experimental investigation of a diode-pumped Tm:$YAlO_3$ laser with *a*- and *b*-cut crystal orientations," IEEE J. Sel. Top. Quantum Electron. **11**(3), 674–681 (2005).
12. K. Mizutani, T. Itabe, S. Ishii, M. Aoki, K. Asai, A. Sato, H. Fukuoka, T. Ishikawa, and K. Noda, "Diode-pumped 2 µm pulse laser with noncomposite Tm,Ho:YLF rod conduction-cooled down to −80 °C," Appl. Opt. **54**(26), 7865–7869 (2015).
13. J. Qiao, S. Zhao, K. Yang, W. Song, W. Qiao, C. Wu, J. Zhao, G. Li, D. Li, T. Li, H. Liu, and C. Lee, "High-quality 2 µm Q-switched pulsed solid-state lasers using spin-coating-coreduction approach synthesized Bi_2Te_3 topological insulators," Photonics Res. **6**(4), 314–320 (2018).
14. Y. Lin, P. Lee, J. Xu, C. Wu, C. Chou, C. Tu, C. Tu, M. Chou, and C. Lee, "High-pulse-energy topological insulator Bi_2Te_3-based passive Q-switched solid-state laser," IEEE Photonics J. **8**(4), 1–10 (2016).
15. H. Lee, K. Kim, and H. Kim, "Pulse-amplitude equalization of rational harmonic mode-locked fiber laser using a semiconductor optical amplifier loop mirror," Opt. Commun. **160**(1-3), 51–56 (1999).
16. G. Martin, T. J. Siemers, and J. R. Thompson, "Modeling structural features of pulse timing jitter in a single-mode, Q-switched, Nd:YAG laser," Laser Phys. **27**(8), 085005 (2017).
17. D. C. Hanna, B. Luther-Davies, H. N. Rutt, and R. C. Smith, "A two-step Q-switching technique for producing high power in a single longitudinal mode," Opt. Quantum Electron. **3**(4), 163–169 (1971).
18. D. C. Hanna, B. Luther-Davies, and R. C. Smith, "Active Q-switching technique for producing high laser power in a single longitudinal mode," Electron. Lett. **8**(15), 369–370 (1972).
19. D. C. Hanna and Y.-W. J. Koo, "Stable single-mode operation of a Q-switched laser by a simple resonator length control technique," Opt. Commun. **43**(6), 414–418 (1982).
20. O. Svelto, *Principles of Lasers* (Springer, 2010), 5th ed.
21. Y. Sato and T. Taira, "Spectroscopic properties of neodymium-doped yttrium orthovanadate single crystals with high-resolution measurement," Jpn. J. Appl. Phys. **41**(Part 1, No. 10), 5999–6002 (2002).
22. O. A. Buryy, D. Y. Sugak, S. B. Ubizskii, I. I. Izhnin, M. M. Vakiv, and I. M. Solskii, "The comparative analysis and optimization of the free-running Tm^{3+}:YAP and Tm^{3+}:YAG microlasers," Appl. Phys. B **88**(3), 433–442 (2007).
23. W. Koechner, *Solid-State Laser Engineering* (Springer, 2006), sixth ed.
24. I. F. Elder and J. Payne, "Diode-pumped, room-temperature Tm:YAP laser," Appl. Opt. **36**(33), 8606–8610 (1997).
25. H. Kalaycioglu, A. Sennaroglu, and A. Kurt, "Influence of doping concentration on the power performance of diode-pumped continuous-wave Tm^{3+}:$YAlO_3$ lasers," IEEE J. Sel. Top. Quantum Electron. **11**(3), 667–673 (2005).
26. J. Dong and K. Ueda, "Longitudinal-mode competition induced instabilities of Cr^{4+},Nd^{3+}: $Y_3Al_5O_{12}$ self-Q-switched two-mode laser," Appl. Phys. Lett. **87**(15), 151102 (2005).
27. C. Bollig, W. A. Clarkson, and D. C. Hanna, "Stable high-repetition-rate single-frequency Q-switched operation by feedback suppression of relaxation oscillation," Opt. Lett. **20**(12), 1383–1385 (1995).